Multitracing Capability of Double-Scattering Compton Imager With NaI(Tl) Scintillator Absorber

Hee Seo, *Student Member, IEEE*, Chan Hyeong Kim, *Member, IEEE*, Jin Hyung Park, Jong Kyung Kim, Ju Hahn Lee, Chun Sik Lee, Soo Mee Kim, and Jae Sung Lee, *Member, IEEE*

***Abstract*—The Compton camera can provide 3-D images of radioactive material distribution based on a single measurement at a fixed position. The Compton camera also can image several different kinds of radioactive materials simultaneously, by means of the "multitracing" capability. In the present study, this multitracing capability was tested for a double-scattering-type Compton camera, or Double-Scattering Compton Imager (DOCI), which utilizes two double-sided silicon strip detectors (DSSDs) and one NaI(Tl) scintillation detector. Our experimental result shows that the ^{137}Cs and ^{60}Co gamma sources can be clearly distinguished in 2-D and 3-D Compton images, and that there is no significant interference between the two gamma sources. The imaging resolutions were determined to be 6.2 and 4.7 mm FWHM for the ^{137}Cs (662 keV) and ^{60}Co (1332 keV) point sources at 4 cm, respectively. The angular resolutions, determined from the angular resolution measure (ARM) distributions, were 7.3° and 6.5° for the source energies of 662 and 1332 keV, respectively. The DOCI remains under development; its imaging resolution will be further improved with the incorporation of more sophisticated detectors and the related electronics, including a faster scintillation detector (LYSO) and higher-spatial-resolution position-sensitive detectors.**

***Index Terms*—Compton camera, double-scattering, multitracing, NaI(Tl) scintillator.**

I. Introduction

THE "MULTITRACING" capability, which makes possible the simultaneous monitoring of different kinds of radioactive materials, is one of the most advantageous characteristics of the Compton camera. This capability was first demonstrated using a Compton camera composed of two segmented germanium detectors for the scatterer and absorber detectors by Yang *et al.* [1]. Recently, they replaced the component detectors with two double-sided strip germanium detectors, and, then, demonstrated the multitracing capability for biological samples (soybean and mouse) [2], [3].

Manuscript received June 19, 2009; revised August 14, 2009 and October 06, 2009; accepted October 23, 2009. Date of current version June 16, 2010. This work was supported in part by the Nuclear R&D Program in Korea through BAERI and Basic Research Program and in part by the Korean Ministry of Knowledge Economy (2008-P-EP-HM-E-06-0000)/Sunkwang Atomic Energy Safety Co., Ltd.

H. Seo, C. H. Kim, J. H. Park, and J. K. Kim are with the Department of Nuclear Engineering, Hanyang University, Seoul 133-791, Korea (e-mail: chkim@hanyang.ac.kr).

J. H. Lee and C. S. Lee are with the Department of Physics, Chung-Ang University, Seoul 156-756, Korea.

S. M. Kim and J. S. Lee are with the Department of Nuclear Medicine and Interdisciplinary Program in Radiation Applied Life Science, Seoul National University, Seoul 110-744, Korea.

Color versions of one or more of the figures in this paper are available online at http://ieeexplore.ieee.org.

Digital Object Identifier 10.1109/TNS.2009.2035806

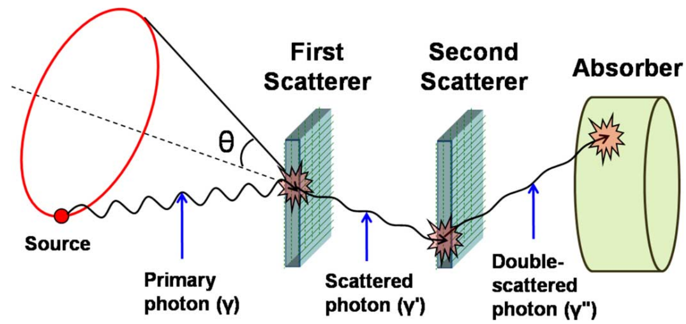

Fig. 1. Principle of DOCI. The photon emitted from the source must have interactions with these three component detectors in order to be recorded as an effective event suitable for use in image reconstruction. The axis of a backprojected cone is determined from the interaction positions in the scatterer detectors, whereas the half-angle (θ) of the cone is determined from the deposited energy in the first scatterer detector. The intersections of three or more cones will indicate the location of the source.

In the present study, the multitracing capability was tested for a double-scattering-type Compton camera, or Double-Scattering Compton Imager (DOCI). The DOCI, which was developed mainly for industrial applications [4] and security inspection [5], offers a very high imaging resolution. The DOCI uses two scatterer detectors, instead of one as in the case of the conventional single-scattering-type Compton camera, and determines the trajectory of gamma-rays very accurately, maximizing the imaging resolution.

To test the multitracing capability of the Compton camera, two pointlike gamma sources, ^{137}Cs and ^{60}Co, were placed close to each other, the Compton image being obtained for that source combination. The acquired 2-D and 3-D images were then examined for imaging resolution and also for any possible interference between the two gamma sources.

II. DOCI

A. Imaging Principle

The DOCI consists of three radiation detectors, two position-sensitive scatterer detectors and one absorber detector (Fig. 1). The scatterer detectors determine the trajectory of a scattered photon between them, which trajectory becomes the axis of the backprojected cone. The absorber detector is placed directly behind the second scatterer detector to determine the energy of the double-scattered photon, used for energy gating to reject random-coincidence events. The scattering angle, which is the half-angle (θ) of the cone, is calculated by Compton kinematics from the energy deposited in the first scatterer detector. The 3-D

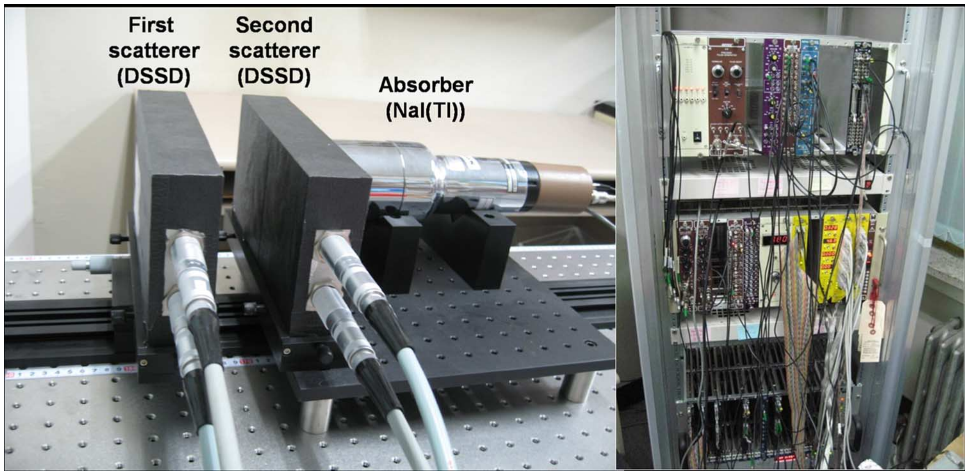

Fig. 2. Prototype DOCI composed of two double-sided silicon strip detectors (DSSDs) as scatterer detectors and one NaI(Tl) scintillation detector as absorber detector.

location of a gamma-ray source can be determined by the intersections of three or more backprojected cones. The purpose of the DOCI is to maximize the imaging resolution; this is achieved by using high-spatial-resolution scatterer detectors to minimize the uncertainty in the determination of the interaction positions [6].

B. System Overview

In the prototype DOCI, two identical double-sided silicon strip detectors (DSSDs) are used as the first and second scatterer detectors, and one NaI(Tl) scintillation detector is utilized as the absorber detector (Fig. 2). NIM and CAMAC modules are employed to handle the multichannel signals from the component detectors. Triple-coincidence logic is applied to the three component detectors in order to exclusively record events with interaction times falling within a predefined coincidence window (= 300 ns in the present study). The component detectors are calibrated for time, with respect to the coincidence unit, using a pulse generator. When the trigger signals from all of the component detectors are within the 300 ns coincidence window, a gate signal is generated and fed into a 16-channel peak-sensing analog-to-digital converter (ADC) (model: Phillips 7164) to open the gate. To provide enough time to digitize analog signals in the ADC, a veto signal of 30μs duration is fed into the coincidence unit and a look-at-me (LAM) signal, a signal that is sent to the CAMAC controller to initiate the transfer of the digitized data to the PC, is delayed by 30 μs with respect to the gate signal. Finally, an in-house ROOT-based program [7] is used to monitor and control the data acquisition (DAQ) system.

To prevent electromagnetic interference, each DSSD is placed in a light-tight aluminum box. An optical breadboard is used to precisely align the detectors. The first scatterer detector is mounted on a precision rail system so that its position can be changed as necessary. The distance between the second scatterer detector and the absorber detector is fixed at 1 cm.

C. Scatterer Detectors

Two identical DSSDs (model: W1(DS), Micron Semiconductor, U.K.) determine the trajectory of the gamma-rays by measuring the interaction positions and deposited energies of the Compton scatterings. The DSSDs are 5 cm $\times$ 5 cm $\times$ 0.15 cm in dimension, with 16 strips on each side. The interaction position resolution is, therefore, about 0.3 cm $\times$ 0.3 cm $\times$ 0.15 cm. The DSSDs are made of low-Z material (silicon), showing a low degree of Doppler broadening and a high Compton-to-total ratio in gamma-ray interaction. Note that because the Doppler broadening in Compton scattering is considered to be the theoretical limit of the imaging resolution of a Compton camera [8], [9], the atomic number of the scatterer detector material is one of the most important decision parameters.

Four MUX-16s manufactured by mesytec GmbH & Co. (Germany) handle the multichannel signals from the scatterer detectors. In a MUX-16, the preamplified signal is split and fed into the shaping amplifier and the leading-edge discriminator. The same threshold level is applied to all of the 16 leading edge discriminators. The DOCI receives the signals from only one strip, even though a MUX-16 produces up to two output signals whose amplitudes are above the threshold level and whose interaction times are within 50 ns. The output signals from a MUX-16 are the energy and position signals from an interaction, the amplitude of a position signal being coded in 20 mV increments per channel (= per strip).

Each of the strips in the DSSDs was energy-calibrated separately, because the gains slightly differed from one another (difference: $<10\%$). The energy resolutions of the strips in the DSSDs were determined to be on the order of 5% for the photon energies of interest (50–500 keV). The total leakage current, which is the summed leakage current from the 16 strips, was about 5 μA at room temperature. The discrimination level was set at $\sim$40 keV to eliminate noise signals.

D. Absorber Detector

A 3 inch diameter $\times$ 3 inch height NaI(Tl) scintillation detector (model: 905-4, ORTEC, U.S.) was used as the absorber detector in the DOCI to determine the energy of the double-scattered photon. The absorber detector is used only for energy gating, which imposes a gating condition such that, for an effective event, the sum of the deposited energies in the three component detectors should match the source energy within a

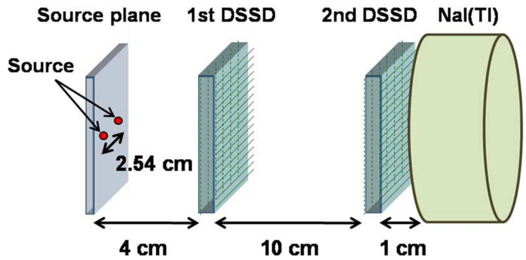

Fig. 3. Experimental setup.

given margin ($\pm 10\%$ of the source energies used in the present study). The signal from the absorber was preamplified in a photomultiplier tube (PMT) base with a preamplifier (model: 276, ORTEC, U.S.), and then split into two paths, i.e., for energy and timing. To obtain the energy information, the preamplified signal was fed into an amplifier (model: 572A, ORTEC, U.S.) with 1 μs shaping time, and then digitized in the ADC. To obtain the timing information, the preamplified signal was fed into a timing filter amplifier (model: 474, ORTEC, U.S.) with 20 ns of integration and differentiation times, and subsequently fed into a constant fraction discriminator (CFD, model: 935, ORTEC, U.S.) to generate a trigger signal. The measured energy resolution of the absorber detector was 9 keV at the 59.5 keV peak of ^{241}Am, and 77 keV at the 1332 keV peak of ^{60}Co. The discrimination level of the absorber detector was $\sim$10 keV.

III. Multitracing Capability

A. Experimental Setup

The three component detectors were placed in parallel as shown in Fig. 2. The distance between the first and second scatterer detectors was 10 cm. Two pointlike gamma sources (diameter: $\sim$1 mm) ^{137}Cs (662 keV) and ^{60}Co (1173 and 1332 keV), were placed 4 cm in front of the DOCI. The distance between these two sources was 2.54 cm (Fig. 3). The activities of the sources were 9.41 μCi and 9.98 μCi, respectively. The triple-coincidence data were collected for 12 h.

B. ^{137}Cs and ^{60}Co Imaging

A total of 71 985 events were recorded after applying the triple-coincidence logic to the component detectors; the count rate was 1.7 counts/s. The coincidence timing resolution was about 170 ns, which was measured by using a time-to-digital converter (TDC) for the time difference of interactions in the component detectors. The sum-energy spectrum, which is the sum of the photon energies measured by the three component detectors, is shown in Fig. 4. Three peaks corresponding to the source energies of 662, 1173, and 1332 keV, respectively, can be seen. Two-dimensional energy gating was employed to effectively reject random coincidence events. Fig. 5 shows the two-dimensional energy spectrum and the energy gates employed. The x-axis represents the sum of the energies deposited in the first and second scatterer detectors, whereas the y-axis represents the energy deposited in the absorber detector. The sum-energy gates were 662 $\pm$66 keV, 1173 $\pm$117 keV, and 1332 $\pm$133 keV, representing $\pm$10% of the source energies. As shown in Fig. 5, there are a number of random coincidence events which is mainly due to the fact that the DSSDs are relatively noisy and the timing resolution is poor. Due to the same reasons, the horizontal lines are shown around the source energies, which occur when the triple-coincidence requirement is satisfied with the noise triggers of the DSSDs and the full-energy absorption event in the absorber detector. The events below $\sim$200 keV in the absorber detector are mainly the backscattering peak and the natural background events. If the random events are in the 2-D energy gate by chance, it was used in the image reconstruction. However, if the geometrical interpretation is used, the random events in the 2-D energy gate could be further rejected by the use of the limitation on the possible scattering angle.

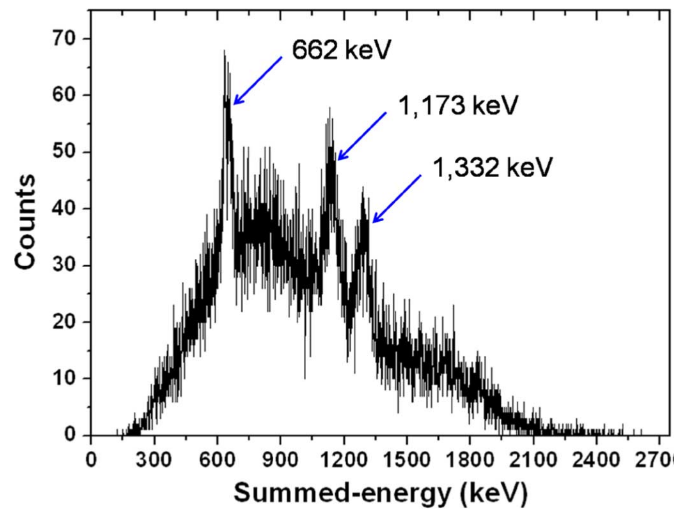

Fig. 4. Sum-energy spectrum of Compton camera measured in triple coincidence with three component detectors for ^{137}Cs (662 keV) and ^{60}Co (1173 and 1332 keV) sources.

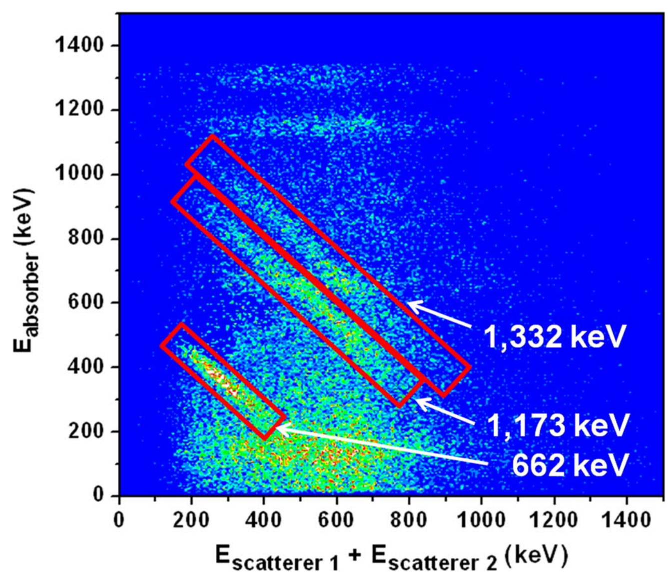

Fig. 5. Two-dimensional energy spectrum and energy gates used in present study for ^{137}Cs and ^{60}Co sources. The three diagonals indicate that the sum of the deposited energies in the component detectors is a value close to the source energies of 662, 1173, and 1332 keV.

Fig. 6 shows the energy spectra of (a) the first scatterer detector, (b) the second scatterer detector, (c) the absorber detector, and (d) the sum of a, b, and c for the source energies of (upper) 662 keV, (middle) 1173 keV, and (bottom) 1332 keV after the

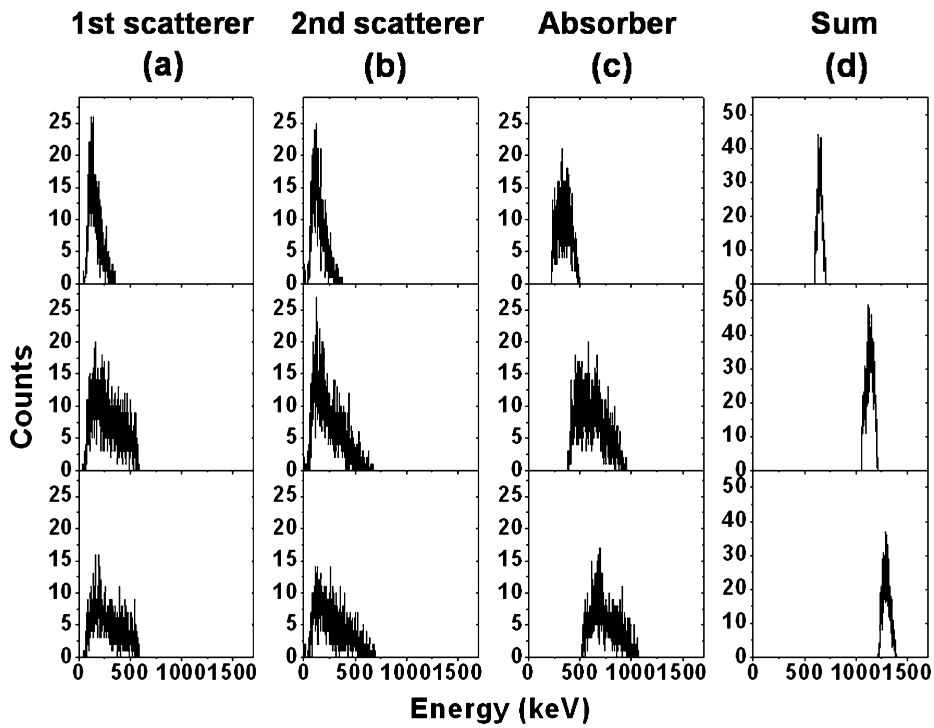

Fig. 6. Gated energy spectra for (a) first scatterer detector, (b) second scatterer detector, (c) absorber detector, and (d) sum of a, b, and c for source energies of (upper) 662 keV, (middle) 1173 keV, and (bottom) 1332 keV. The energy resolutions of the sum-energy peak (d) for 662 keV, 1173 keV, and 1332 keV were determined to be 65.4, 98.7, and 94.6 keV FWHM, respectively.

2-D energy gates were applied. The energy resolutions of the sum-energy peaks [Fig. 6(d)] were determined to be 65.4, 98.7, and 94.6 keV FWHM for 662, 1173, and 1332 keV, respectively. The numbers of effective events were 2215, 3776, and 2605 for the 662 keV, 1173 keV, and 1332 keV gammas, respectively. The imaging sensitivity, defined as the number of effective events divided by the number of gamma-rays emitted from the source, was calculated as 1.73×10^{-7} (662 keV), 2.37×10^{-7} (1173 keV), and 1.63×10^{-7} (1332 keV). The measured imaging sensitivity has a similar value $(\sim 10^{-7})$ with the result of our previous Monte Carlo simulation study [10]. Compared with a single-scattering-type Compton camera, the imaging sensitivity of the DOCI is rather low ($\sim$10% or less) due to the requirement of the double-scattering within two thin-scatterer detectors; however, we have focused on the improvement of the imaging resolution by accurately determining the trajectory of the scattered photon, which becomes an axis of the backprojected cone (Fig. 1). The imaging sensitivity could be easily improved by using a multiple number of scatterer detectors as well as position-sensitive absorber detector. Fig. 7 shows the distributions of the scattering angles for (a) the 662 keV, (b) 1173 keV, and (c) 1332 keV source energies. The scattering angles were limited by the discrimination level of the first scatterer detector as well as the geometrical configuration of the two scatterer detectors. The minimum values of the scattering angles were 26.6°, 14.5°, and 12.7° for the 662 keV, 1173 keV, and 1332 keV source energies, respectively.

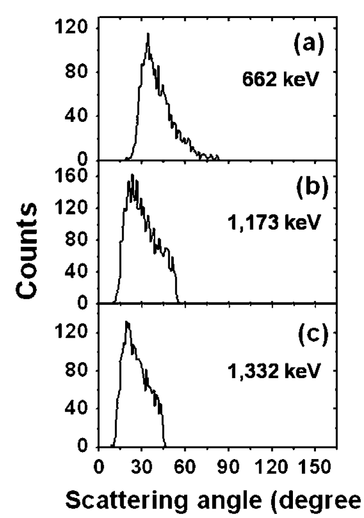

Fig. 7. Distributions of scattering angles for source energies of (a) 662 keV, (b) 1173, and (c) 1332 keV. The scattering angle is limited by the discrimination level of the first scatterer detector as well as the geometrical configuration of the scatterer detectors.

Fig. 8 shows the reconstructed Compton images and the projections for (a) the 662 keV, (b) 1173 keV, (c) 1332 ke, and (d) all of them. The images were reconstructed using the list-mode maximum likelihood expectation maximization (MLEM) algorithm [11], [12] with five iterations. The MLEM algorithm is widely used for reconstructing the Compton images and evaluating the performance of the imaging system. The list-mode MLEM is considered to be more suitable for Compton imaging reconstruction than the conventional EM method due to calculation efficiency; that is, the number of events is much smaller than the number of possible detection bins. The distance between the

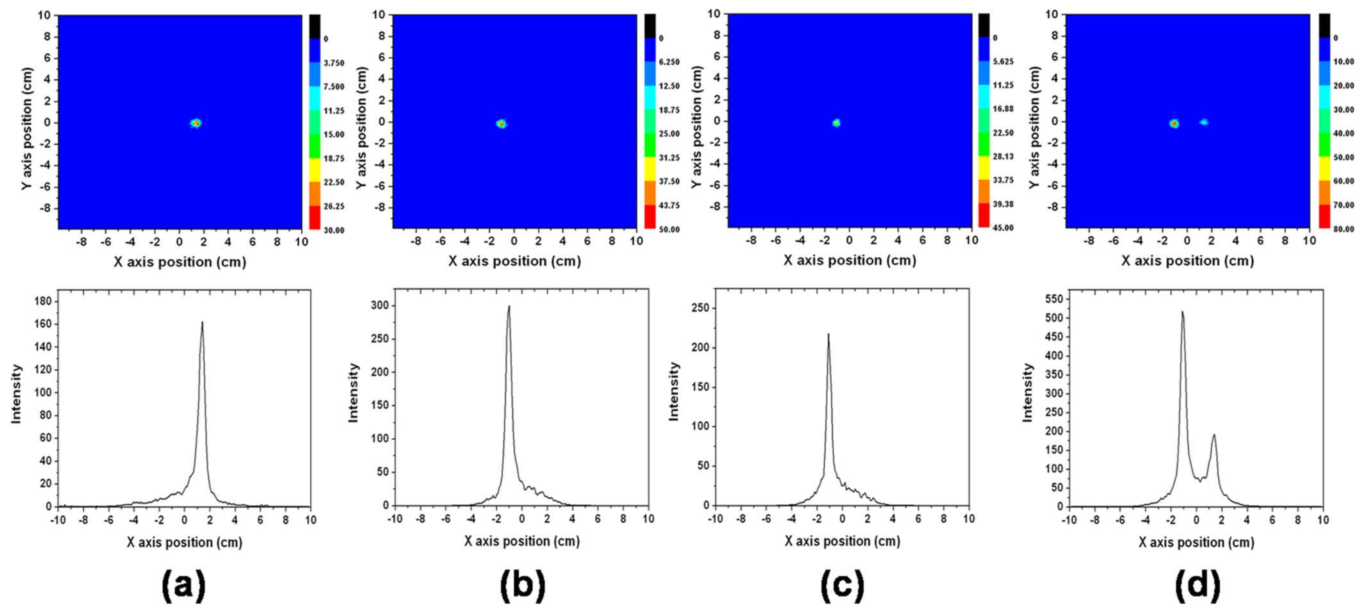

Fig. 8. Reconstructed Compton images and their projections for (a) 662 keV, (b) 1173 keV, (c) 1332 keV, and (d) all of them. The imaging resolutions for 662, 1173, and 1332 keV were determined to be 6.2, 5.7, and 4.7 mm FWHM, respectively.

two sources evaluated by the peak positions in the projection was 2.4 cm, which was very close to the true value (=2.54 cm). There was no significant interference between the two sources. Fig. 9 shows that the 3-D locations of multiple radioisotopes can be simultaneously imaged by a single measurement at a fixed position. The imaging resolution was determined to be 6.2, 5.7, and 4.7 mm FWHM for the 662 keV, 1173 keV, and 1332 keV source energies, respectively (see Fig. 8). It should be noted that the artificially good imaging resolution might be obtained when the MLEM algorithm is used to reconstruct a Compton image for a point source without uniform background due to a nonnegativity constraint [13]. Therefore, the angular resolution measure (ARM) [9], which is defined as the difference between the Compton scattering angles determined from the Compton kinematics and the interaction positions with a known source location, was also obtained. Because the ARM is calculated from the deposited energy and the interaction positions, it is independent of the reconstruction algorithm, appropriately showing the performance of the Compton imaging system. As shown in Fig. 10, the ARM distributions have non-Gaussian shapes; hence, the Voigt function which is a convolution of the Gaussian distribution and the Lorentzian distribution was used to fit the ARM distributions and obtain the FWHM values [14], [15]. The angular resolutions determined as the FWHM's of the ARM distributions were 7.3°, 6.7°, and 6.5° for the source energies of 662, 1173, and 1332 keV, respectively. The asymmetry shown at the tail of the ARM distributions mainly comes from the random coincidence events and the off-axis source location.

Note that the imaging resolution as well as the angular resolution was improved with the source energy, which is due mainly to the fact that the effect of Doppler broadening is reduced and the energy resolution is improved with the increase of the source energy. For a low-energy gamma source (e.g., 140 keV ^{99m}Tc), the Doppler broadening significantly affects the imaging resolution of a Compton camera, whereas, for a high-energy gamma source (e.g., >500 keV), the improvement of the energy resolution plays more important role on the imaging resolution. For this reason, our result, which shows higher imaging resolution for the higher energy source, mainly comes from the improvement of the energy resolution.

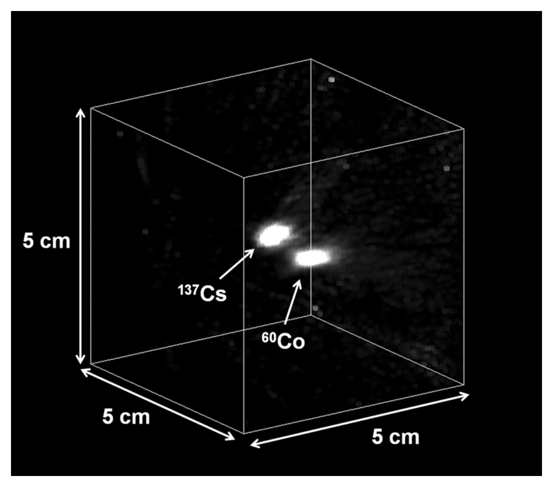

Fig. 9. Three-dimensional Compton image of ^{137}Cs and ^{60}Co pointlike sources. The image was taken from a single measurement at a fixed position.

IV. Conclusion

In the present study, the multitracing capability of a double-scattering-type Compton camera, or Double-Scattering Compton Imager), was tested. The result was very promising: the ^{137}Cs and ^{60}Co pointlike gamma sources were clearly distinguished in the 2-D and 3-D Compton images, and there was no significant interference between the two gamma sources. The imaging resolutions were determined to be 6.2 and 4.7 mm FWHM for the ^{137}Cs (662 keV) and ^{60}Co (1332 keV)

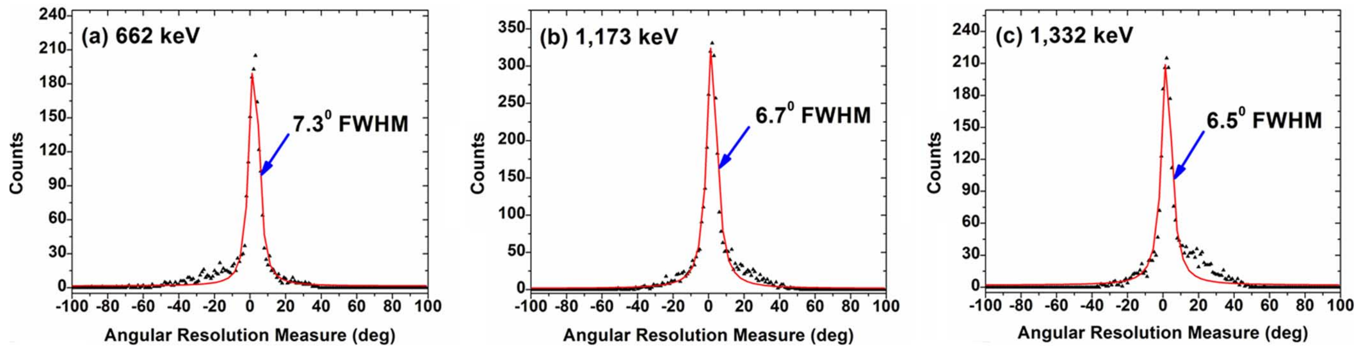

Fig. 10. Angular resolution measure (ARM) distributions with fitted Voigt functions for source energies of (a) 662 keV, (b) 1173 keV, and (c) 1332 keV.

sources at 4 cm, respectively. The angular resolutions, determined from the ARM distributions, were 7.3° and 6.5° for the source energies of 662 and 1332 keV, respectively. The limiting factor of the current system on the imaging resolution is the spatial resolution of the DSSDs [6]. Our simulation study [16] shows that the imaging resolution could be improved by $\sim$20% by improving the spatial resolution of the first scatterer detector from 3 mm to 1 mm strip pitch for the source energy of 511 keV.

The DOCI remains under development; its imaging resolution and imaging sensitivity will be further improved with the incorporation of more sophisticated detectors and data acquisition electronics. First, the NaI(Tl) absorber detector will be replaced with a much faster LYSO ($Lu_{1.8}Y_{0.2}SiO_5$) scintillation detector. This upgrade will reduce random coincidences and thereby improve both the imaging resolution and the imaging sensitivity. The count rate in the absorber detector dramatically increases with the increase of the source activity due to its high detection efficiency. The increase of count rate increases random coincidence events, some of which are not filtered out by the 2-D energy gate, and, consequently, degrade the imaging resolution. Therefore, a faster absorber detector is advantageous for a better imaging resolution as well as an improved imaging sensitivity. The scatterer detectors will be exchanged for very-high-spatial-resolution (760 μm strip pitch) silicon strip detectors. The NIM/CAMAC-based data acquisition electronics will eventually be exchanged for a low-noise ASIC/ADC, which is currently under development. We believe that these improvements will significantly enhance the imaging resolution and imaging sensitivity of the DOCI, which undoubtedly will find many practical applications in both the industrial and medical fields. For example, the DOCI could be used to determine the 3-D distribution of radioactive contamination in a concrete shield of a nuclear facility, which is crucial information for decommissioning and radiation safety.

REFERENCES

[1] Y. F. Yang, Y. Gono, S. Motomura, S. Enomoto, and Y. Yano, "A Compton camera for multitracer imaging," *IEEE Trans. Nucl. Sci.*, vol. 48, no. 3, pp. 656–661, Jun. 2001.

[2] S. Motomura, S. Enomoto, H. Haba, K. Igarashi, Y. Gono, and Y. Yano, "Gamma-ray Compton imaging of multitracer in biological samples using strip germanium telescope," *IEEE Trans. Nucl. Sci.*, vol. 54, no. 3, pp. 710–717, Jun. 2007.

[3] S. Motomura, Y. Kanayama, H. Haba, Y. Watanabe, and S. Enomoto, "Multiple molecular simultaneous imaging in a live mouse using semiconductor Compton camera," *J. Anal. Atom. Spectrom.*, vol. 23, pp. 1089–1092, 2008.

[4] A. Al-Ghamdi and X. G. Xu, "Estimating the depth of embedded contaminants from in-situ gamma spectroscopic measurements," *Health Phys.*, vol. 84, no. 5, pp. 632–636, 2003.

[5] G. P. Gilfoyle and J. A. Parmentola, "Using nuclear materials to prevent nuclear proliferation," *Sci. Global Secur.*, vol. 9, pp. 81–92, 2001.

[6] H. Seo, S. H. An, J. K. Kim, and C. H. Kim, "Monte Carlo study of a double-scattering Compton camera with GEANT4," *Nucl. Instrum. Meth. A*, vol. 580, pp. 314–317, 2007.

[7] R. Brun and F. Rademakers, "ROOT—An object oriented data analysis framework," *Nucl. Instrum. Meth. A*, vol. 389, pp. 81–86, 1997.

[8] C. E. Ordonez, A. Bolozdynya, and W. Chang, "Doppler broadening of energy spectra in Compton cameras," in *Proc. IEEE Nuclear Science Symp. Conf. Rec.*, 1998, vol. 2, pp. 1361–1365.

[9] A. Zoglauer and G. Kanbach, "Doppler broadening as a lower limit to the angular resolution of next generation Compton telescopes," in *Proc. SPIE*, 2003, vol. 4851, pp. 1302–1309.

[10] H. Seo, S. H. Lee, C. H. Kim, S. H. An, J. H. Lee, and C. S. Lee, "Optimal geometrical configuration of a double-scattering Compton camera for maximum imaging resolution and sensitivity," *Nucl. Instrum. Meth. A*, vol. 591, pp. 80–83, 2008.

[11] S. J. Wilderman, J. A. Fessler, N. H. Clinthorne, J. W. LeBlanc, and W. L. Rogers, "Improved modeling of system response in list mode EM reconstruction of Compton scatter camera images," *IEEE Trans. Nucl. Sci.*, vol. 48, no. 1, pp. 111–116, Jan. 2001.

[12] T. Hebert, R. Leahy, and M. Singh, "Three-dimensional maximum likelihood reconstruction for an electronically collimated single photon-emission imaging system," *J. Opt. Soc. Amer. A*, vol. 7, no. 7, pp. 1305–1313, 1990.

[13] J. W. LeBlanc *et al.*, "^{99m}Tc imaging performance of the C-SPINT Compton camera," in *1999 IEEE Nuclear Science Symp. Conf. Rec.*, vol. 1, pp. 545–552.

[14] S. Takeda *et al.*, "A new Si/CdTe semiconductor Compton camera developed for high-angular resolution," in *Proc. SPIE*, 2007, vol. 6706, pp. 67060S-1–67060S-11.

[15] J. J. Olivero and R. L. Longbothum, "Empirical fits to the Voigt line width: A brief review," *J. Quant. Spectrosc. Radiat. Transf.*, vol. 17, no. 2, pp. 233–236, 1997.

[16] H. Seo, S. H. Lee, C. H. Kim, J. H. Lee, C. S. Lee, and J. S. Lee, "Monte Carlo study for first scatterer detector of double-scattering Compton imager," in *Proc. 5th Korea-Japan Joint Meeting on Medical Phys.*, 2008, p. 209.